STScI | SPACE TELESCOPE SCIENCE INSTITUTE

Instrument Science Report ACS 2019-04

SBC Time-Dependent Sensitivity and L-flats

R.J. Avila, M. Chiaberge, D. Kossakowski, J. Averbukh, S. Lockwood

September 16, 2019

Abstract

The time-dependent and spatial sensitivities of the SBC detector on ACS were measured using observations of the calibration star cluster NGC6681. The sensitivity of the detector declined by up to $\sim 9\%$ *since launch, with a rate of* $\sim 0.5\%$*/year since 2007. New calibration files (*`IMPHTTAB`*) were produced, and will be included in the calibration pipeline in order to properly update the photometric zeropoints of every FLT image. The low-frequency L-flats were derived by directly fitting 2D polynomial surfaces to the spatial sensitivity data. The resulting products are smoother than the previous versions, due to the different method of deriving the flats. The corrections in the flats are on the order of* $\pm 8\%$*. The overall photometric accuracy is 2.5% (except for F165LP which is 3.3%), after combining the low-frequency L-flats with the high-frequency P-flats to make new LP-flats, and applying the new TDS corrections.*

1 Introduction

The Solar Blind Channel (SBC) on the Advanced Camera for Surveys (ACS) is a Multi-Anode Microchannel Array (MAMA) photon counting device. It is optimized for observations in the far-ultraviolet (FUV) regime from 1150 to 1700Å, with a field of view of $35'' \times 31''$, and a plate scale of $\sim 0.032''$/pix. It is equipped with a set of six imaging filters (five long-pass and one Lyα filter) and two low-resolution prisms.

Measuring temporal changes in the sensitivity of the detector is straightforward. The same target should be observed over time and its flux measured. If the target is not intrinsically variable then any changes in brightness are due to sensitivity changes in the imaging system. Using a star cluster yields measurements of many stars at once that can be combined for more robust statistical analysis. Mack et al. (2005) measured the time-dependent sensitivity (TDS) of the detector for the first 3 years of operations. There are now 17 years worth of observations, covering the entire on-orbit lifetime of the instrument.

Obtaining an L-flat for this detector is difficult because flat field illumination in this wavelength range is not available neither in the lab nor in space. While the high-frequency pixel-to-pixel variations (P-flats) can be determined for all filters by using deuterium lamp images (Bohlin et al., 1999; Avila et al., 2016), the L-flats need to be derived by using dithered observations of stellar fields. By placing the same stars at different positions on the detector and measuring their relative changes in brightness, the spatial variation of the sensitivity of the detector can be determined.

The current L-flat was derived by Mack et al. (2005) using observations of star cluster NGC6681. The L-flat was derived by binning up photometric measurements of stars into a 16×16 'chess-board' so that the L-flat is determined for a pixelized version of the detector. The 'chess-board' was then smoothed using a Gaussian kernel. Bohlin and Mack (2006) later found evidence that these flats were too lumpy. This was due to the sparse number of observations available at the time, which left bins without any observations in their grid. In this work the L-flats are derived again from scratch in order to eliminate the lumpiness of the present flats.

Section 2 presents the data used, provides an explanation of how basic image calibration was performed, and how the catalog of stars was generated. Section 3 describes the initial derivation of the TDS. Section 4 presents the derivation of the L-flats and the final derivation of the TDS. Section 5 summarizes this report and presents a discussion of the results. Section 6 discusses the technical aspects of how these results are being implemented.

2 Data

The ACS science instrument team has used the open cluster NGC6681 (Figure 1) as a calibration field for the SBC since launch. It was chosen because it contains a suitably dense number of UV-bright point sources. All of the SBC images of this field that are available in the Mikulski Archive for Space Telescopes[1] (MAST) were downloaded in raw format. Failed observations were discarded. Additionally, any observations where the average detector temperature exceeded 25°C were also discarded in order to remove images with high dark current, which is difficult to correct for in SBC data (Avila, 2017). The final list of the images used can be found in Table 1. The observations also sample a range of instrument temperatures and exposure times.

To define the astrometric grid, it would be ideal to align the SBC images directly to the *Gaia* (Gaia Collaboration et al., 2018) reference frame. There is not much overlap between the SBC images and the GAIA catalog because of the small size of the SBC footprint, and because GAIA does not contain many UV-bright sources. SBC images were aligned to

[1] `https://mast.stsci.edu`

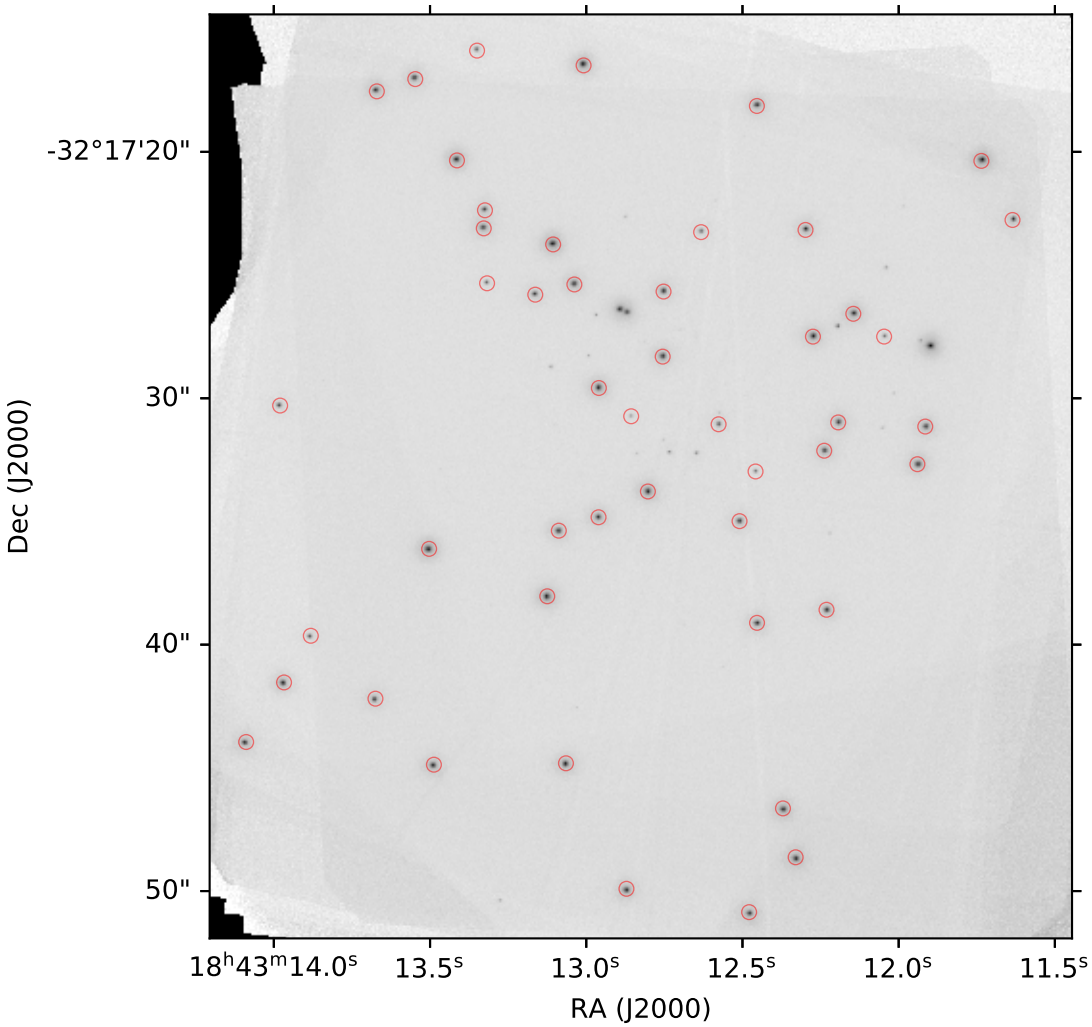

Figure 1: Image of the cluster using all the available F115LP images. The circles mark all the stars in the final photometry catalog. The size of the circles is equivalent to the size of the photometry apertures, which were 12 pixel (0.3″) in radius. North is up and east is to the left.

Gaia by first aligning near-UV images (F275W) taken with WFC3/UVIS to GAIA and then aligning the SBC images to the WFC3/UVIS observations. The WFC3 images were from GO-13297 (PI: Piotto), visits 94 and 95.

The initial calibration of the images was done using the standard CALACS pipeline (version 10.1.0), but using a flat field image that only contained the high-frequency P-flat component. Avila et al. (2016) noted that the high-frequency structure in the P-flat changed in 2007, and therefore which calibration file is used depends on the observation date. For images taken before Feb 20, 2007, `p5p1513pj_pfl.fits` was used. `36h2201nj_pfl.fits` was used on images taken after that date.

Table 1: Archive rootname of all the files used in this study.

F115LP	F125LP	F140LP	F150LP	F165LP
j8c803htq	j8c803huq	j8c803hvq	j8c803hwq	j8c803hyq
j8c804wmq	j8c601rwq	j8c804woq	j8c804wpq	j8c804wxq
j8ep01ufs	j8c601s2q	j8ep01uhs	j8bu52t0q	j8ep01ujs
j8eg01hbq	j8c601s4q	j8eg01hdq	j8bu52t1q	j8eg01hfq
j8eg01hkq	j8bu01k5q	j8eg01hiq	j8bu52t2q	j8eg01hgq
j8ep02uxq	j8bu01k7q	j8ep02uzq	j8bu52taq	j8ep02v1q
j8ep03gkq	j8bu01kaq	j8ep03gmq	j8bu52tbq	j8ep03goq
j8ep04lsq	j8bu01kfq	j8ep04luq	j8bu52tdq	j8ep04lwq
j8eg02wbq	j8bu01kiq	j8eg02wdq	j8bu52teq	j8eg02wfq
j8eg02wkq	j8bu01klq	j8eg02wiq	j8bu52umq	j8eg02wgq
j8ep05pnq	j8bu01koq	j8ep05ppq	j8bu52unq	j8ep05prq
j8ep06hpq	j8bu01ktq	j8ep06hrq	j8bu52uoq	j8ep06htq
j8eg03n3q	j8bu01kvq	j8eg03n5q	j8ep01uis	j8eg03n7q
j8eg03ncq	j8c804wnq	j8eg03naq	j8eg01heq	j8eg03n8q
j8ep07vgq	j8ep01ugs	j8ep07viq	j8eg01hhq	j8ep07vkq
j8ep08meq	j8eg01hcq	j8ep08mgq	j8ep02v0q	j8ep08miq
j8hv01m2q	j8eg01hjq	j8hv01m4q	j8ep03gnq	j8hv01m6q
j8hv02eyq	j8ep02uyq	j8hv02f0q	j8ep04lvq	j8hv02f2q
j8hv05cuq	j8ep03glq	j8hv05cwq	j8eg02weq	j8hv05cyq
j8hv06qtq	j8ep04ltq	j8hv06qvq	j8eg02whq	j8hv06qxq
j8hv07p4q	j8eg02wcq	j8hv07p6q	j8ep05pqq	j8hv07p8q
j8hv08sjq	j8eg02wjq	j8hv08slq	j8ep06hsq	j8hv08snq
j8hv09yxq	j8ep05poq	j8hv09yzq	j8eg03n6q	j8hv09z1q
j8hv10ckq	j8ep06hqq	j8hv10cmq	j8eg03n9q	j8hv10coq
j8hv11a7q	j8eg03n4q	j8hv11a9q	j8ep07vjq	j8hv11abq
j8hv12dxq	j8eg03nbq	j8hv12dzq	j8ep08mhq	j8hv12e1q
j8vb01okq	j8ep07vhq	j8vb01omq	j8hv01m5q	j8vb01ooq
j8vb03egq	j8ep08mfq	j8vb03eiq	j8hv02f1q	j8vb03ekq
j8vb05zjq	j8hv01m3q	j8vb05zlq	j8hv05cxq	j8vb05znq
j8vb07f1q	j8hv02ezq	j8vb07f3q	j8hv06qwq	j8vb07f5q
j95ua1k2q	j8hv05cvq	j95ua1k4q	j8hv07p7q	j95ua1k6q
j95ua2itq	j8hv06quq	j95ua2ivq	j8hv08smq	j95ua2ixq
j9i003lrq	j8hv07p5q	j9i003lvq	j8hv09z0q	j9i003lzq
j9i003lsq	j8hv08skq	j9i003lwq	j8hv10cnq	j9i003m6q
j9i004jaq	j8hv09yyq	j9i004jeq	j8hv11aaq	j9i004jiq
j9i004jbq	j8hv10clq	j9i004jfq	j8hv12e0q	j9i004jjq
j9v602jqq	j8hv11a8q	j9v602juq	j8vb01onq	j9v602jyq
j9v602jrq	j8hv12dyq	j9v602jvq	j8vb03ejq	j9v602jzq
j9v603o7q	j8vb01olq	j9v603obq	j8vb05zmq	j9v603ofq
j9v603o8q	j8vb03ehq	j9v603ocq	j8vb07f4q	j9v603ogq
j9v607kgq	j8vb05zkq	j9v607kkq	j95ua1k5q	j9v607koq
j9v607khq	j8vb07f2q	j9v607klq	j95ua2iwq	j9v607kpq
j9v604ljq	j95ua1k3q	j9v604lnq	j9i003lxq	j9v604lrq
j9v604lkq	j95ua2iuq	j9v604loq	j9i003lyq	j9v604lyq
ja4o01xuq	j9i003ltq	ja4o01xyq	j9i004jgq	ja4o01y2q
ja4o01xvq	j9i003luq	ja4o01xzq	j9i004jhq	ja4o01y3q
ja4o02aeq	j9i004jcq	ja4o02aiq	j9v602jwq	ja4o02amq
ja4o02afq	j9i004jdq	ja4o02ajq	j9v602jxq	ja4o02anq
jbbe02hbq	j9v602jsq	jbbe02hfq	j9v603odq	jbbe02hjq
jbbe02hcq	j9v602jtq	jbbe02hgq	j9v603oeq	jbbe02hkq
jbbe04ihq	j9v603o9q	jbbe04ilq	j9v607kmq	jbbe04ipq
jbbe04iiq	j9v603oaq	jbbe04imq	j9v607knq	jbbe04iqq
jbnw01qbq	j9v607kiq	jbnw01qfq	j9v604lpq	jbnw01qjq
jbnw01qcq	j9v607kjq	jbnw01qgq	j9v604lqq	jbnw01qkq
jbuq01lkq	j9v604llq	jbuq01loq	ja4o01y0q	jbuq01lsq
jbuq01llq	j9v604lmq	jbuq01lpq	ja4o01y1q	jbuq01ltq
jc6e01eoq	ja4o01xwq	jc6e01esq	ja4o02akq	jc6e01eyq
jc6e01epq	ja4o01xxq	jc6e01etq	ja4o02alq	jc6e01ezq
jcfw01zrq	ja4o02agq	jcfw01zwq	jbbe02hhq	jcfw01a1q
jcfw01zsq	ja4o02ahq	jcfw01zxq	jbbe02hiq	jcfw01a3q
jcs601bpq	jbbe02hdq	jcs601btq	jbbe04inq	jcs601bxq
jcs601bqq	jbbe02heq	jcs601buq	jbbe04ioq	jcs601byq
jd0j01o0q	jbbe04ijq	jd0j01o6q	jbnw01qhq	jd0j01ocq
jd0j01o1q	jbbe04ikq	jd0j01o7q	jbnw01qiq	jd0j01ofq
jd4b01ilq	jbnw01qdq	jd4b01ipq	jbuq01lqq	jdp301m7q
jd4b01imq	jbnw01qeq	jd4b01iqq	jbuq01lrq	jdp301m8q
jdp301lzq	jbuq01lmq	jdp301m3q	jc6e01euq	jduc01luq
jdp301m0q	jbuq01lnq	jdp301m4q	jc6e01exq	jduc01lwq
jduc01liq	jc6e01eqq	jduc01lqq	jcfw01zyq	
jduc01lnq	jc6e01erq	jduc01lrq	jcfw01zzq	
	jcfw01zuq		jcs601bvq	
	jcfw01zvq		jcs601bwq	
	jcs601brq		jd0j01o8q	
	jcs601bsq		jd0j01obq	
	jd0j01o2q		jd4b01irq	
	jd0j01o3q		jd4b01isq	
	jd4b01inq		jdp301m5q	
	jd4b01ioq		jdp301m6q	
	jdp301m1q		jduc01lsq	
	jdp301m2q		jduc01ltq	
	jduc01loq			
	jduc01lpq			

The source list was created by making a full drizzled stack of the F115LP images and running it through the DAOStarFinder task, part of the PHOTUTILS python package (Bradley et al., 2016), setting a detection threshold 50σ above the background. The list was further culled by removing stars that were less than $0.5''$ away from any other star. The final list, containing 48 stars, was used to perform the photometry throughout the rest of this study. Figure 1 shows the cluster with the 48 stars marked.

Table 2: WCS parameters used to make the drizzled products.

Parameter	**Value**
Size X	1400 pix
Size Y	1500 pix
Pixel scale	$0.025''$/pixel
CRVAL1	280.8034387 deg
CRVAL2	-32.29254762 deg

3 Time-Dependent Sensitivity

The analysis for the TDS was done first. The calibrated and aligned images (FLT files) were sorted into groups, based on filter and observation dates. Images with the same filter and observation date were drizzled together, and the same world coordinate system (WCS) was used for all drizzled products (Table 2). Photometry was performed on each drizzled image using the aperture_photometry task of PHOTUTILS. Tests of different aperture sizes showed that apertures with a radius of $0.3''$ produced the smallest scatter in the relative flux measurements of each star. Any photometric measurement that contained bad pixels inside the aperture was thrown out. Bad pixels are defined as pixels with zero weight in the drizzled product. Apertures corrections were not applied because this study pertains to relative, and not absolute, fluxes.

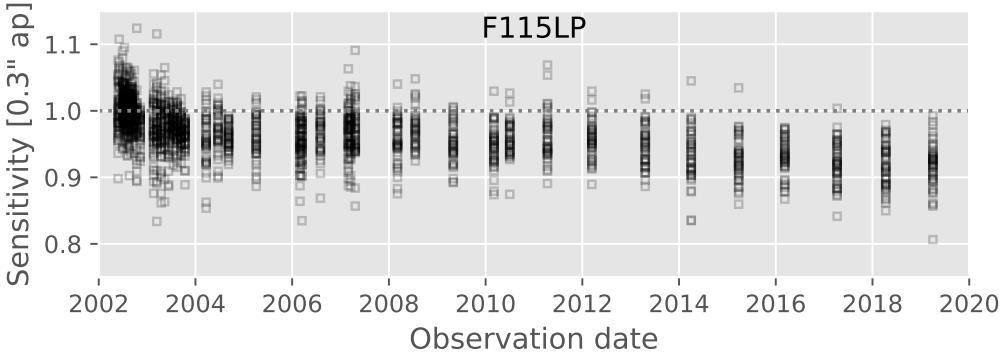

Figure 2: Sensitivity measurements as a function of time for the F115LP filter. Each box represents a measurement for an individual star. The number of boxes per date varies, as some stars may not have valid data on a given date.

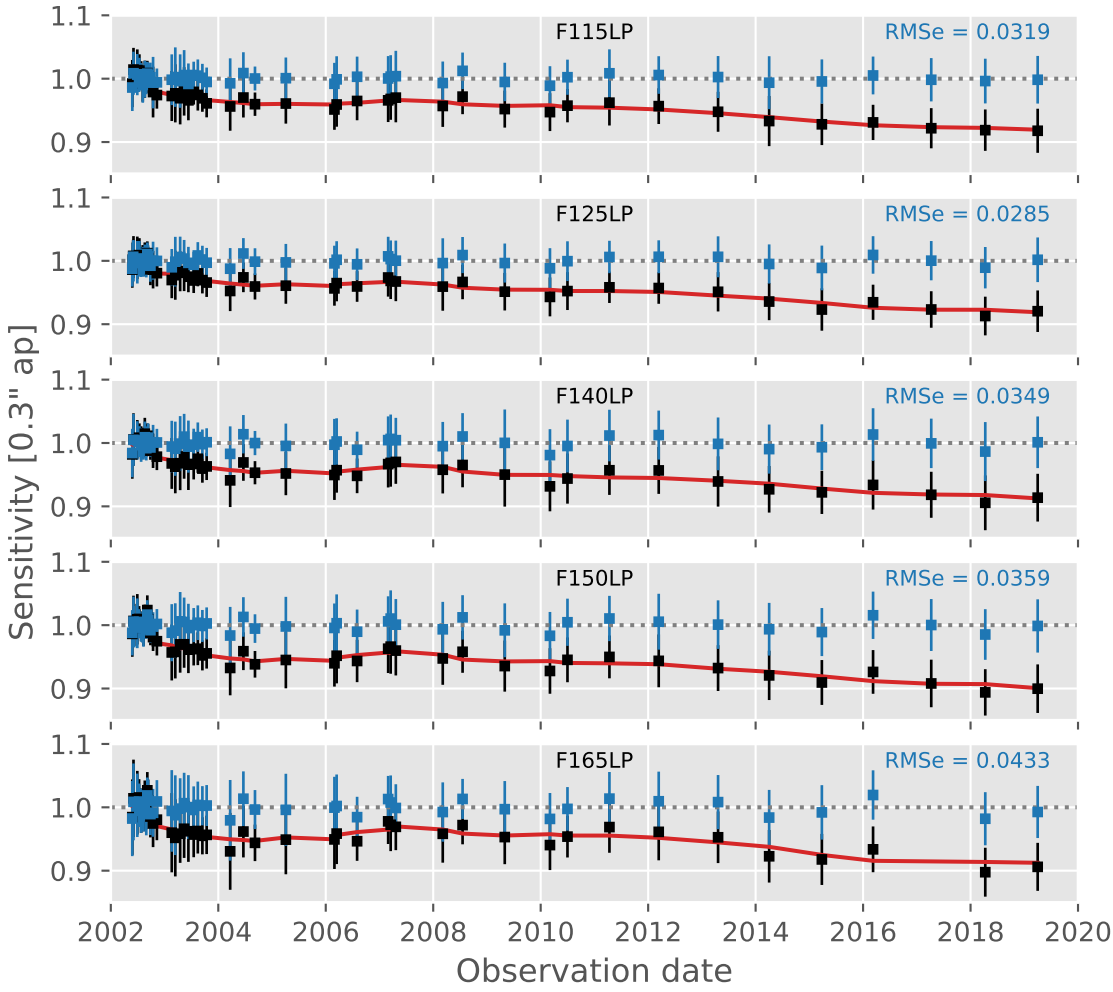

Figure 3: Initial sensitivity measurements for each filter in this study. Black boxes are the mean and standard deviation of the sensitivity before any TDS correction. The red line is the extracted TDS. Blue boxes are the sensitivity after applying TDS correction.

A master table containing every photometric measurement for every star was made, one table per filter. Each row in the table represents one star, while each column corresponds to an observation date. A reference flux for each star needs to be defined because the sensitivity of the detector is constantly changing. The reference flux of each star was defined as the mean flux of the star during the first six months of SBC operations (May 2002 – November 2002). Each individual star measurement was normalized by the reference flux for that star, which converted the table into TDS measurements. Figure 2 shows how each individual star measurement differs from the reference flux over time for the F115LP filter, presented so that readers can visualize how much scatter is present in the sensitivity data at this point in the analysis. The scatter within each observation set comes from Poisson noise and the lack of L-flat calibration. In Figure 3, the black boxes correspond to the mean sensitivity at each observation date, and the error bars are the standard deviation. Each panel of the figure corresponds to one of the five filters in this study.

A rolling box average of 5 time periods was applied to the sensitivity measurements (red line in Figure 3). That TDS was then applied to the individual measurements of each star, and the mean and standard deviation of observations for each date was re-derived (blue boxes and error bars). The residual RMS of the corrected measurements is shown in blue text in each filter panel. These values are the residuals of the individual measurements and not of the means (blue boxes).

4 L-flats

Measurements of a star need to be taken at many different locations on the detector in order to derive an L-flat. Every FLT image was drizzled individually, as opposed to making a stack for each date, because dithers were used in every observation. Photometry was again performed on the drizzled versions of the images, and a record of the location of each star in each of the corresponding FLT images was kept. Another table was made containing the count rates, FLT pixel location, and observation date of each star. Using the observation date, the TDS correction derived in the previous step was applied to each measurement, and the mean count rate for each star derived. Each individual star measurement was normalized to the mean count rate of the star. These spatial sensitivity measurements were cleaned up by removing stars that were 3σ away from the overall sigma-clipped mean. Table 3 lists the number of measurements used to derive the L-flat for each filter.

Table 3: Number of stellar measurements per filter used to derive L-flat.

Filter	**Number of images**	**Total measurements**
F115LP	69	2966
F125LP	81	3268
F140LP	69	2993
F150LP	79	3184
F165LP	67	2913

Figure 4 shows the deviation from the mean for every photometric measurement in the F115LP, as a function of position on the detector. The Astropy (The Astropy Collaboration et al., 2018) models and fitting packages were used to generate and fit polynomial, Legendre, and Chebyshev functions of orders 3, 4, and 5 to the 2D scatter data. 2D polynomials of 3rd order were found to have the best combination of minimizing the scatter without letting the corners of the flat fields deviate by large amounts. With the polynomial coefficients derived, FITS versions of the L-flats were generated where the mean of a box 100×100 pixels in size, centered on pixel (510,510), was used to normalize the entire image. This normalization scheme is similar to what was used to normalize the current L-flats (Mack et al., 2005).

The final, normalized curves are the L-flats. Figure 5 shows both the previously derived and new L-flats for comparison. Both sets appear qualitatively similar, but the new L-flats are smoother than the old L-flats, due to the method used to derive them. The newly derived

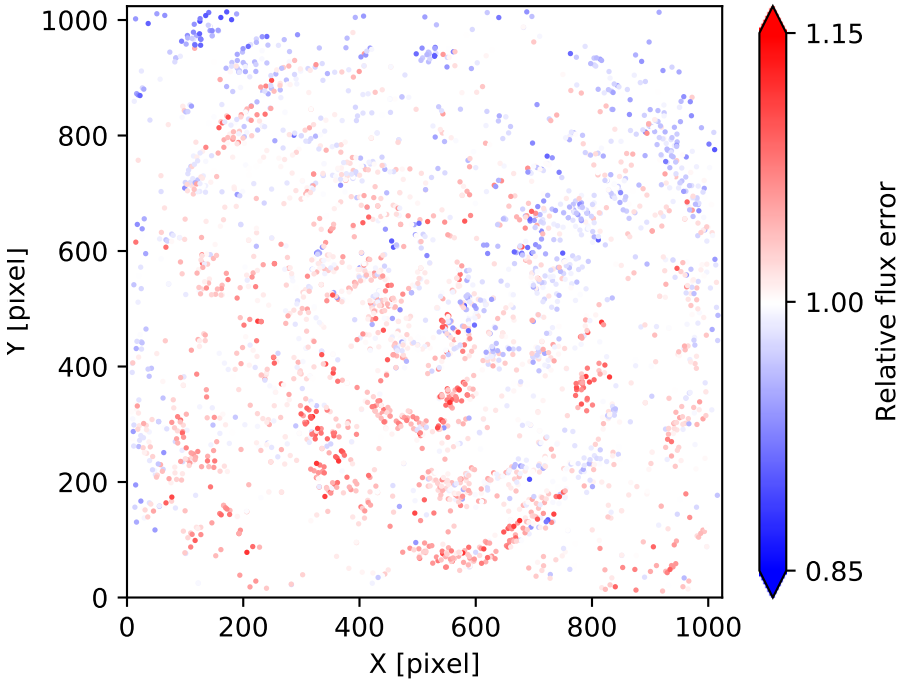

Figure 4: Relative flux error as a function of position on the detector. Red points are measurements that were higher than the mean, blue were lower.

L-flats were combined with the appropriate P-flats to produce new LP-flats for use in the calibration pipeline.

4.1 Re-deriving the Time-Dependent Sensitivity

The TDS was derived again, using the newly derived LP-flats. The RAW images were calibrated using the new flats, and the drizzling and photometry were performed in the exact same way as the first iteration of the TDS derivation in section 3.

Figure 6 shows the updated TDS and corrected photometry. As in Figure 3, the blue boxes and error bars shows the final sensitivity measurements. The residual RMS of the corrected measurements is shown in blue text in each filter panel.

5 Discussion

Previous analysis shows that the sensitivity decreased sharply during the first 1.6 years of operation and then flattened out, as shown in Figure 8 in Mack et al. (2005). At that time it was unclear whether the sensitivity would remain stable or decline again. Now that there are 15 more years worth of data, that question can be re-visited. The initial decline in sensitivity was followed by a slight upturn that lasted until mid-2007, although this increase was still within the error bars of the measurements. It is not known why the detector sensitivity

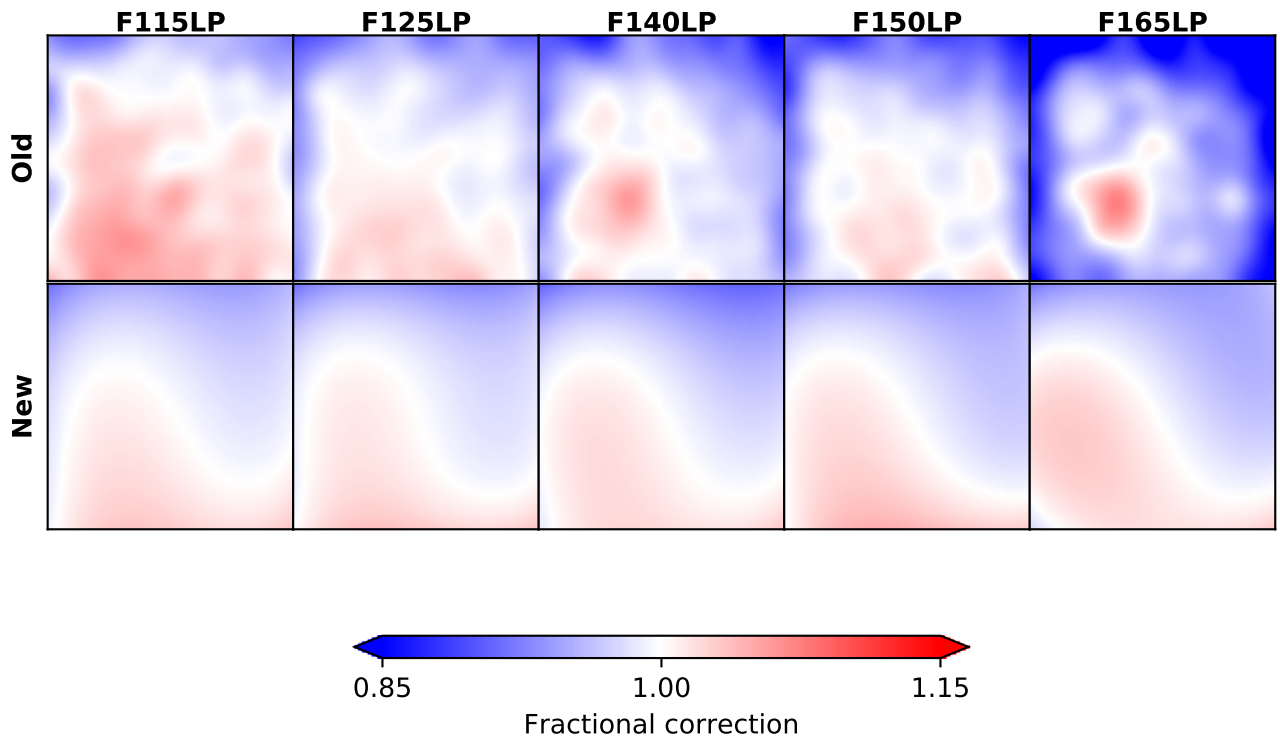

Figure 5: The old and new L-flat frames. The colors indicate the L-flat contribution to the fractional correction that is applied when an image is divided by the LP-flat. All images are presented with the same stretch.

would increase as it did in between 2004 and 2007, and the upturn does not match with any of the major camera events (electronics box failure, side-switch, CCD operating temperature change, etc.) that occurred in that time. Since 2007, the sensitivity of the detector has been slowly declining from ∼97% to ∼91% in 2019.

Table 4 summarizes the residual RMS of the sensitivity measurements when using only the P-flat, and when using the LP-flat. Both sets include the TDS correction. The final corrections result in photometry accurate to within 2.5%, except F165LP where it is 3.3%.

Table 4: Residual RMS of the sensitivity measurements depending on which flat was used (TDS included).

Filter name	**Using P-flat (%)**	**Using LP-flat (%)**
F115LP	3.19	2.50
F125LP	2.85	2.10
F140LP	3.49	2.40
F150LP	3.59	2.42
F165LP	4.33	3.30

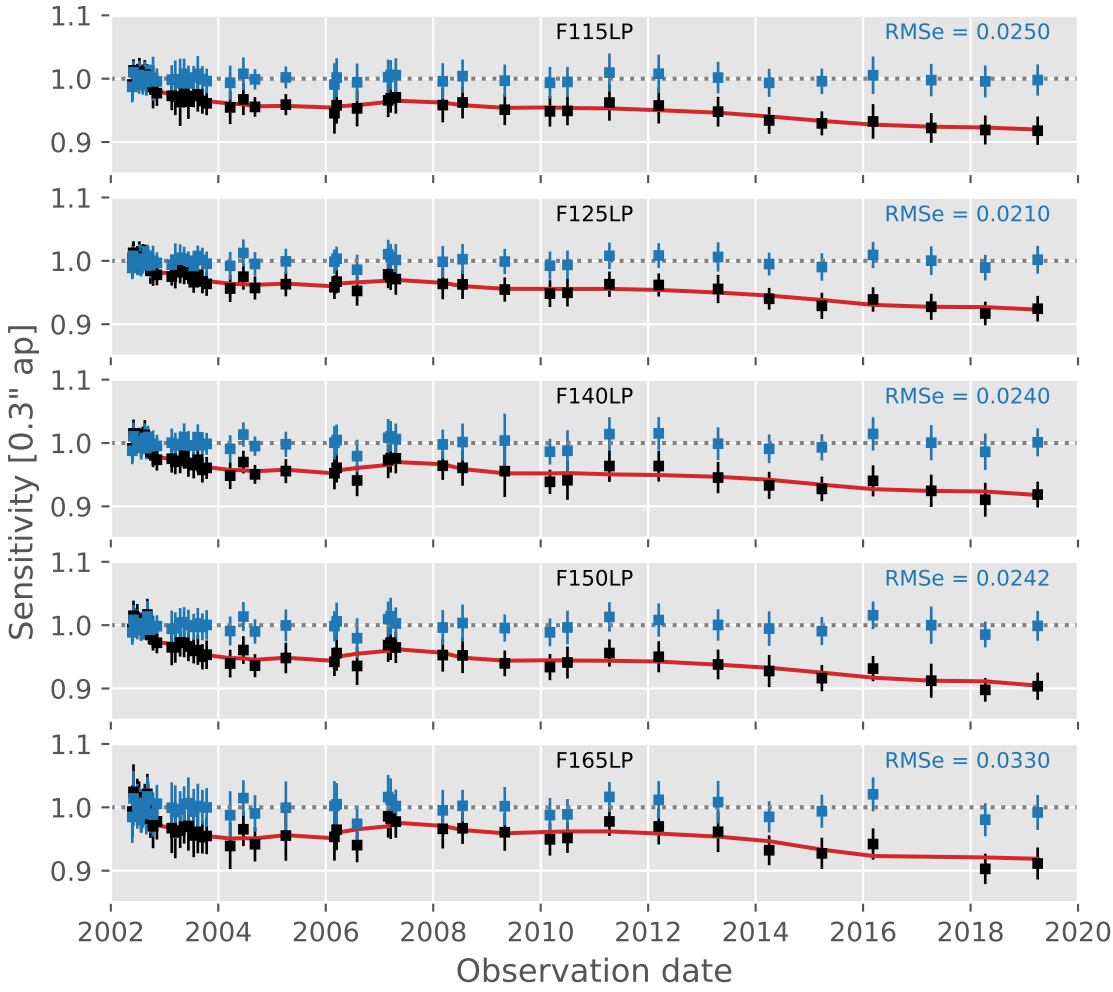

Figure 6: Final sensitivity measurements. Black boxes are the mean and standard deviation of the sensitivity before any TDS correction. The red line is the extracted TDS. Blue boxes are the sensitivity after applying TDS correction.

5.1 Temperature dependence

Mack et al. (2005) noted that the sensitivity of the SBC shows a slight dependence on the temperature of the detector at the time of the observation. The SBC does not have temperature sensors on the detector, but the temperature of the electronics box, just on top of the detector, is used as a proxy. This temperature is recorded at the beginning and end of each exposure and is reported in the `MDECODT1` and `MDECODT2` header keywords. The average temperature of these two values is used as the temperature measurement. The SBC temperature remains between 12°C and 14°C while the detector is turned off. Once turned on, the detector begins warming up and it is recommended that observations not be taken when the detector is $\gtrsim 25$°C because the dark rate increases significantly above that temperature (Avila, 2017).

Figure 7 shows how the sensitivity changes as a function of temperature. An error weighted fit to the data shows that there is a loss of sensitivity of $0.11 \pm 0.03\%$ per degree.

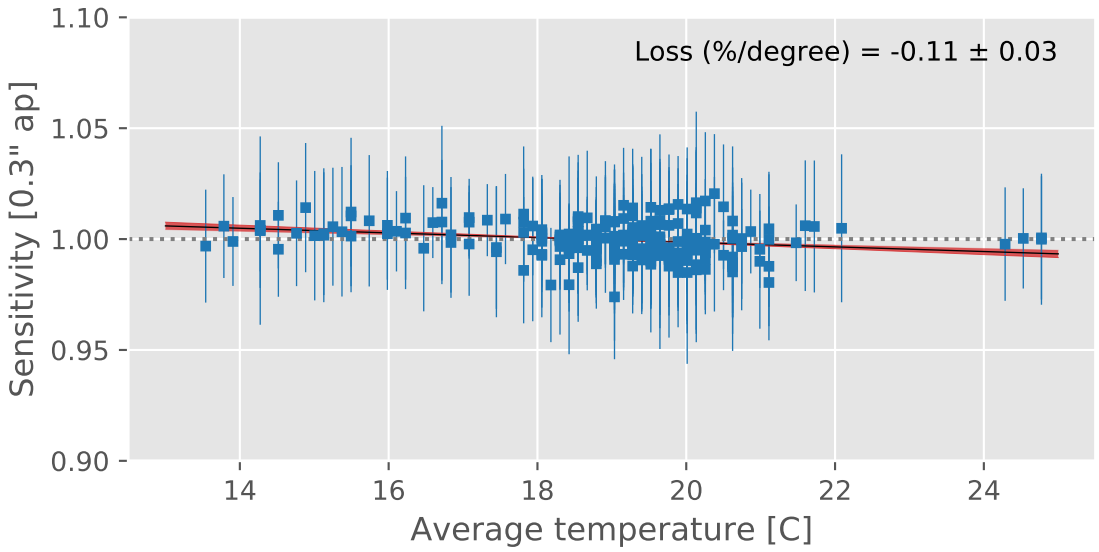

Figure 7: Sensitivity with respect to detector temperature at time of observation. These points include the TDS correction. All filters are included in this plot.

Because the temperature dependence is within the scatter of the sensitivity measurements, corrections for this effect have been left out of the pipeline. More observations are needed where the detector temperature is between 22°C and 24°C to try to understand whether this effect is real or if the fit is being driven by the large number of measurements between $\sim$ 19°C to 21°C. The UV Contamination Monitor program has been modified to enable this investigation.

6 Implementation

As reported by Avila et al. (2016), two sets of P-flats are now necessary for the SBC; one set to be used for observations taken before February 2007 and another for after that date. The L-flats are combined with the two sets of P-flats to make the final LP-flats to be delivered to the pipeline. A total of 10 files were delivered to the Calibration Reference Data System[2] (CRDS) in June 2019 to be used in the pipeline. SBC images in MAST have been re-processed using these new LP-flats, so these changes should be transparent to users downloading images from this date on.

The TDS is implemented in the pipeline via a reference file called `IMPHTTAB`. This file contains the inverse sensitivity values (`PHOTFLAM`), as a function of date. RAW images calibrated using the CALACS pipeline will have their `PHOTFLAM` header keyword populated with the appropriate value for the observation date. Users should normalize the images to a common zeropoint if they intend to combine observations from different dates.

For new observations taken after the latest sensitivity measurements, the TDS will be extrapolated using the last 2 data points. Since the TDS is derived using a rolling window, at any given point in time, the final two points of the TDS correction don't contain full

[2] `https://hst-crds.stsci.edu`

Table 5: LP-flat delivered for use in the pipeline.

Filter	Pre-2007	Post-2007
F115LP	36h2200sj_pfl.fits	36h2200gj_pfl.fits
F125LP	36h2200kj_pfl.fits	36h2201rj_pfl.fits
F140LP	36h22016j_pfl.fits	36h2200oj_pfl.fits
F150LP	36h2201aj_pfl.fits	36h2201jj_pfl.fits
F165LP	36h2201ej_pfl.fits	36h22012j_pfl.fits

information from monitoring. The sensitivity is not expected to change by more than the scatter in the sensitivity over two years. Any extrapolation within the next year of that, can be assumed to be within the error bars.

Acknowledgements

We would like to thank Jennifer Mack for her useful discussions on this project. We also thank the following ACS Team member for reviewing this work: Tyler Desjardins, Nimish Hathi, Nathan Miles, Yotam Cohen, Melanie Olaes, Ralph Bohlin, and Norman Grogin.

This work has made use of data from the European Space Agency (ESA) mission *Gaia* (`https://www.cosmos.esa.int/gaia`), processed by the *Gaia* Data Processing and Analysis Consortium (DPAC, `https://www.cosmos.esa.int/web/gaia/dpac/consortium`). Funding for the DPAC has been provided by national institutions, in particular the institutions participating in the *Gaia* Multilateral Agreement.

This work also made use of the following software packages: `ipython` (Pérez and Granger, 2007), `numpy` and `scipy` (van der Walt et al., 2011), `pandas` (McKinney, 2010), and `matplotlib` (Hunter, 2007).

References

R. J. Avila. Updated Measurements of ACS/SBC Dark Rates. Technical Report ISR ACS 2017-04, Space Telescope Science Institute, May 2017.

R. J. Avila, M. Chiaberge, and R. Bohlin. SBC Internal Lamp P-flat Monitoring. Technical Report ISR ACS 2016-02, Space Telescope Science Institute, March 2016.

R. C. Bohlin and J. Mack. SBC Flats: Prism P-Flats and Imaging L-Flats. Technical Report ISR ACS 2006-08, Space Telescope Science Institute, December 2006.

R. C. Bohlin, G. Hartig, and G. Meurer. Flats: SBC Data from Thermal Vacuum Testing. Technical Report ISR ACS 1999-02, Space Telescope Science Institute, May 1999.

Larry Bradley, Brigitta Sipocz, Thomas Robitaille, Erik Tollerud, Christoph Deil, Zè Vinícius, Kyle Barbary, Hans Moritz Günther, Azalee Bostroem, Michael Droettboom, Erik Bray, Lars Andersen Bratholm, T. E. Pickering, Matt Craig, Sergio Pascual, Johnny

Greco, Axel Donath, Wolfgang Kerzendorf, StuartLittlefair, Geert Barentsen, Francesco D'Eugenio, and Benjamin Alan Weaver. astropy/photutils v0.2.2, September 2016. URL `https://doi.org/10.5281/zenodo.155353`.

Gaia Collaboration, A. G. A. Brown, A. Vallenari, T. Prusti, J. H. J. de Bruijne, C. Babusiaux, C. A. L. Bailer-Jones, M. Biermann, D. W. Evans, L. Eyer, and et al. Gaia Data Release 2. Summary of the contents and survey properties. *AAP*, 616:A1, August 2018. doi: 10.1051/0004-6361/201833051.

J. D. Hunter. Matplotlib: A 2d graphics environment. *Computing In Science & Engineering*, 9(3):90–95, 2007.

J. Mack, R. Gilliland, R. van der Marel, and R. Bohlin. SBC L-Flat Corrections and Time-Dependent Sensitivity. Technical report, Space Telescope Science Institute, November 2005.

Wes McKinney. Data structures for statistical computing in python. In Stéfan van der Walt and Jarrod Millman, editors, *Proceedings of the 9th Python in Science Conference*, pages 51 – 56, 2010.

Fernando Pérez and Brian E. Granger. IPython: a system for interactive scientific computing. *Computing in Science and Engineering*, 9(3):21–29, May 2007. ISSN 1521-9615. doi: 10.1109/MCSE.2007.53. URL `http://ipython.org`.

The Astropy Collaboration, A. M. Price-Whelan, B. M. Sipőcz, H. M. Günther, P. L. Lim, S. M. Crawford, S. Conseil, D. L. Shupe, M. W. Craig, N. Dencheva, A. Ginsburg, J. T. VanderPlas, L. D. Bradley, D. Pérez-Suárez, M. de Val-Borro, T. L. Aldcroft, K. L. Cruz, T. P. Robitaille, E. J. Tollerud, C. Ardelean, T. Babej, M. Bachetti, A. V. Bakanov, S. P. Bamford, G. Barentsen, P. Barmby, A. Baumbach, K. L. Berry, F. Biscani, M. Boquien, K. A. Bostroem, L. G. Bouma, G. B. Brammer, E. M. Bray, H. Breytenbach, H. Buddelmeijer, D. J. Burke, G. Calderone, J. L. Cano Rodríguez, M. Cara, J. V. M. Cardoso, S. Cheedella, Y. Copin, D. Crichton, D. DÁvella, C. Deil, É. Depagne, J. P. Dietrich, A. Donath, M. Droettboom, N. Earl, T. Erben, S. Fabbro, L. A. Ferreira, T. Finethy, R. T. Fox, L. H. Garrison, S. L. J. Gibbons, D. A. Goldstein, R. Gommers, J. P. Greco, P. Greenfield, A. M. Groener, F. Grollier, A. Hagen, P. Hirst, D. Homeier, A. J. Horton, G. Hosseinzadeh, L. Hu, J. S. Hunkeler, Ž. Ivezić, A. Jain, T. Jenness, G. Kanarek, S. Kendrew, N. S. Kern, W. E. Kerzendorf, A. Khvalko, J. King, D. Kirkby, A. M. Kulkarni, A. Kumar, A. Lee, D. Lenz, S. P. Littlefair, Z. Ma, D. M. Macleod, M. Mastropietro, C. McCully, S. Montagnac, B. M. Morris, M. Mueller, S. J. Mumford, D. Muna, N. A. Murphy, S. Nelson, G. H. Nguyen, J. P. Ninan, M. Nöthe, S. Ogaz, S. Oh, J. K. Parejko, N. Parley, S. Pascual, R. Patil, A. A. Patil, A. L. Plunkett, J. X. Prochaska, T. Rastogi, V. Reddy Janga, J. Sabater, P. Sakurikar, M. Seifert, L. E. Sherbert, H. Sherwood-Taylor, A. Y. Shih, J. Sick, M. T. Silbiger, S. Singanamalla, L. P. Singer, P. H. Sladen, K. A. Sooley, S. Sornarajah, O. Streicher, P. Teuben, S. W. Thomas, G. R. Tremblay, J. E. H. Turner, V. Terrón, M. H. van Kerkwijk, A. de la Vega, L. L. Watkins, B. A. Weaver, J. B. Whitmore, J. Woillez, and V. Zabalza. The Astropy Project: Building an inclusive, open-science project and status of the v2.0 core package. *ArXiv e-prints*, January 2018.

Stéfan van der Walt, S. Chris Colbert, and Gaël Varoquaux. The numpy array: a structure for efficient numerical computation. *CoRR*, abs/1102.1523, 2011. URL `http://arxiv.org/abs/1102.1523`.